

Ultrafast reaction dynamics in cluster ions: Simulation of the transient photoelectron spectrum of $I_2^-Ar_n$ photodissociation

J. Faeder and R. Parson^{a)}

JILA, University of Colorado and National Institute of Standards and Technology and Department of Chemistry and Biochemistry, University of Colorado, Boulder, Colorado 80309-0440

(Received 18 September 1997; accepted 4 December 1997)

Combining an effective Hamiltonian model of electronic structure with nonadiabatic molecular dynamics simulations, we calculate the recently measured transient photoelectron spectrum of I_2^- dissociated inside a cluster of argon atoms. We find good agreement between calculated and experimental spectra. The transient spectral shifts reflect the dynamics of both the I_2^- and argon degrees of freedom, revealing pathways and time scales for dissociation, recombination, and vibrational relaxation. © 1998 American Institute of Physics. [S0021-9606(98)03010-4]

I. INTRODUCTION

The photodissociation and recombination of a dihalide ion embedded in a cluster illustrates the crucial role played by the solvent in chemical reactions that involve charged species. In these strongly interacting systems, the solvent does not merely interrupt and redirect motion on the potential energy surfaces of the isolated molecule, it profoundly modifies the surfaces themselves. As the dihalide solute dissociates in an excited state (Fig. 1), the forces exerted on the solute electrons by the solvent molecules become as important as the forces within the solute; both solute and solvent become polarized. This leads to long range forces that can inhibit dissociation in the initially excited state, and to solvent-induced nonadiabatic transitions that can bring about recombination in other electronic states. Finally, the solvent can stabilize the recombined species by dissipating their excess energy.

Dihalide anion photodissociation in clusters has been studied extensively both experimentally¹⁻⁹ and theoretically,¹⁰⁻¹⁵ but several key aspects of the dynamics remain poorly understood. Little is known about the dynamics that take place on the excited state following photoexcitation or about what motions of the solute and solvent are necessary to bring about electronic relaxation and product formation. Full theoretical modeling of these photodissociation reactions is difficult because it requires both a knowledge of the electronic structure of a manifold of states strongly coupled to the many solvent degrees of freedom and a method of computing the complex dynamics on these surfaces. Several groups have recently developed semiempirical Hamiltonians for dihalides¹⁶⁻¹⁸ and dihalide anions^{13,14} interacting with rare gas atoms. The work of Batista and Coker^{13,16,17} has demonstrated the important role of nonadiabatic dynamics on the multiple potential surfaces in these systems following photoexcitation. Nonadiabatic molecular dynamics simulations of I_2^- photodissociation in argon clusters from Coker's group¹³ and confirmed by our group¹⁴ have

achieved good agreement with the experimental photoproduct distributions.⁷ These simulations helped to determine that two previously ambiguous product channels in the experimental mass spectra correspond to recombination of I_2^- in an electronically excited state¹³ and direct ejection of I^- on a single adiabatic potential surface.¹⁴ To obtain a complete picture of the dynamics following I_2^- photodissociation, however, we need a direct link between the simulations and time-resolved measurements.

Neumark and co-workers¹⁹ have recently measured the transient photoelectron spectrum of $I_2^-Ar_6$ and $I_2^-Ar_{20}$. In their experiment, shown in Fig. 1, a 780 nm laser pulse with a width of about 100 fs excites I_2^- to the dissociative A' state, and a subsequent uv pulse detaches an electron, leaving neutral I_2 in a low-lying electronic state. The kinetic energy spectrum of the detached electrons measures the electron affinity of the transient species, serving as a probe of the anion electronic state and its interactions with the local solvent environment. Using this technique, Neumark and co-workers were able to identify the time required for complete dissociation in $I_2^-Ar_6$ and for the recombination of I_2^- into both the X and A states in $I_2^-Ar_{20}$.¹⁹

In this work we extend our previous model¹⁴ to calculate the time-dependent photoelectron spectrum of $I_2^-Ar_6$ and $I_2^-Ar_{20}$. We find good agreement with the experimental spectra and use the model to explore the underlying mechanisms of dissociation, recombination, and relaxation.

II. METHODS

The effective Hamiltonian model used to compute the potential surfaces of the $I_2^-Ar_n$ has been discussed elsewhere¹⁴ and a comprehensive discussion of the model is currently in preparation.²⁰ The Hamiltonian is constructed in the space defined by the lowest six electronic states of bare I_2^- , which are strongly coupled by the argon solvent. The energies and wave functions of these I_2^- states were determined using an *ab initio* calculation with a semiempirical correction for the spin-orbit coupling.²¹ The potential curves used in the model (Fig. 1) were obtained by scaling the *ab initio* curves to reproduce the experimental equilibrium bond

^{a)} Author to whom correspondence should be addressed; Electronic mail: rparson@jila.colorado.edu

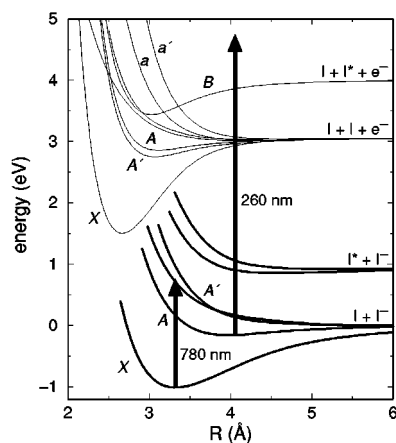


FIG. 1. Femtosecond photoelectron spectroscopy of $I_2^- Ar_n$ photodissociation. A 780 nm pump laser pulse excites I_2^- to the repulsive A' state. The 260 nm probe pulse detaches the excess electron, leaving I_2 in one of its many low-lying electronic states. The probe pulse shown detaches the electron following cluster-induced electronic relaxation of I_2^- to the A state.

distance and well depth for the X state^{19,22} while preserving the *ab initio* energy spacings. The main solute-solvent interaction arises from the induction of electrostatic moments on the argon atoms by the charge distribution of I_2^- . The operator that describes this interaction is computed from the *ab initio* wave functions and the experimental polarizability of argon.^{14,23} The diagonal terms of the operator represent the interaction of the charge distribution of a particular I_2^- state with the polarizable solvent atoms, while the off-diagonal terms contain the coupling between the I_2^- states induced by the solvent. The presence of these terms allows the solvent to polarize the charge distribution on I_2^- , an effect that becomes strong as I_2^- dissociates and the basis states become degenerate.

The electrostatic induction potential dominates both the energetics and the couplings in the system. It is therefore practical to handle the remaining interactions, which arise from dispersion and repulsion, empirically with pairwise Lennard-Jones potentials between the atomic sites. The parameters for the $Ar \cdots Ar$ interaction are chosen to match the experimental values of R_e and D_e for Ar_2 .²⁴ The $I \cdots Ar$ parameters are adjusted so that the potentials reproduce the experimental values of R_e and D_e for $I^- \cdots Ar$ and the three lowest states of $I \cdots Ar$.²⁵ An additional anisotropic $1/R^6$ interaction term is also required to reproduce the state-dependence of the open-shelled $I \cdots Ar$ interaction.^{14,25} Using this procedure ensures that all of the pairwise interactions in the system agree with experimentally determined potentials. The dominant three-body terms in the potential come from the electrostatic induction operator described above.

Simulation of the photoelectron spectrum also requires a model potential for the neutral clusters that result from detaching the electron from I_2^- , leaving I_2 in one of its many low-lying electronic states. In this work we have assumed that the internal potential energy of I_2 is given by the appropriate gas phase potential curve, and the interaction energy is given by the pairwise $I \cdots Ar$ Lennard-Jones potentials used to describe the dispersion and repulsion parts of the $I_2^- \cdots Ar$

interaction.¹⁴ This approximation neglects the state-dependent anisotropic components of the $I \cdots Ar$ interaction,¹⁴ but we are not computing dynamics on the $I_2^- Ar_n$ potential surfaces and the experimental energy resolution is on the order of 100 meV. The electron affinities of $I^- Ar_n$ clusters calculated using the model potentials agree with the experimental values²⁶ to within about 10%. The simulation includes only the lowest ten states of I_2 ,²⁷⁻³⁰ which degrades the accuracy of the simulated spectra below about 0.7 eV in the electron kinetic energy. Three of these states are not known experimentally, but are inferred from an *ab initio* calculation³¹ to be degenerate with either the known a or a' states.³⁰

Using the model Hamiltonian and its derivatives, we simulate photodissociation by running molecular dynamics trajectories augmented by Tully's method^{32,33} for computing hops between the coupled potential surfaces. We mitigate the effects of spurious quantum coherence^{34,35} by resetting the quantum amplitudes periodically in regions where the nonadiabatic coupling is weak.¹⁴ The trajectory results give good agreement with the experimentally observed photoproduct distributions and in a previous work¹⁴ provided mechanisms for all four of the experimentally observed product channels, two of which were ambiguous from the experiments.⁷ The simulations of the photoelectron spectra described below were performed using a single trajectory for bare I_2^- , 21 trajectories started from an ensemble equilibrated to 40 K for $I_2^- Ar_6$, and 81 trajectories started from an ensemble at 50 K for $I_2^- Ar_{20}$. In all three cases, increasing the number of trajectories and raising or lowering the initial temperature has little effect on the simulated spectra.

The time-dependent photoelectron signal at energy E with pump-probe delay Δ is calculated from a quasi-classical golden rule expression,

$$\sigma(E, \Delta) \propto \left\langle \int_{-\infty}^{\infty} dt \exp[-\gamma_{pp}(t-\Delta)^2] \times \sum_f |\mu_{if}(\mathbf{R}(t))|^2 \exp\{-\gamma_d(E)[h\nu - E - (V_{I_2}^f(\mathbf{R}(t)) - V_{I_2}^i(\mathbf{R}(t)))]^2\} \right\rangle, \quad (1)$$

where the angle brackets denote an average over all trajectories, $\mathbf{R}(t)$ is the nuclear configuration at time t , μ_{if} is the transition dipole for detachment of an electron from state i of I_2^- to state f of I_2 , $V_{I_2}^i$ and $V_{I_2}^f$ are the energies of those states, and $h\nu$ is the probe laser energy. This expression is similar in form to the one used by Batista and Coker to simulate the pump-probe signal from I_2 in rare gases matrices.¹⁷ The parameters $\gamma_d(E)$ and γ_{pp} come from the electron detector width and a convolution of the pump and probe laser widths. Because the coordinate dependence of the transition dipoles is unknown, we hold them constant. Simple one-electron selection rules from molecular orbital theory govern which transitions are allowed,^{9,36} however, the large spin-orbit coupling of iodine mixes the electronic configurations to such a high degree^{21,31} that these selection

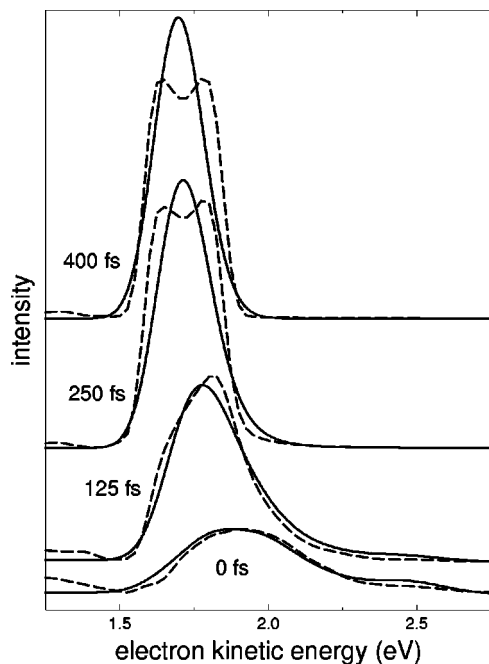


FIG. 2. Time-dependent photoelectron spectra of I_2^- at various pump-probe delay times. Solid lines are simulation results and dashed lines are experimental results from Ref. 9. The full width half maximum convoluted pulse width and detector width are 250 fs and 0.150 eV. The bimodal peaks in the experimental spectra seen at 250 and 400 fs are due to the large solid angle seen by the magnetic bottle photoelectron spectrometer, coupled with an anisotropic electron distribution of the $I^- \rightarrow I$ transition.

rules are valid only for transitions involving the X states of I_2 or I_2^- , which are mixed the least because of their large energetic separations from other states. The dipoles for the one-electron forbidden transitions from the excited states of I_2^- to the X state of I_2 are therefore set to zero, while transition dipoles to all other states of I_2 are set to one. We have also scaled the relative magnitudes of transitions out of the X state of I_2^- in order to reproduce the relative intensities of the

two bands in the $I_2^- Ar_{20}$ spectra that arise from detachment out of the X state. Transition dipoles to the $I_2 X$ state and to the I_2 excited states are set to 12 and 2, respectively.

III. RESULTS AND DISCUSSION

As a test of the simulation method, we have calculated the time-dependent photoelectron spectrum of bare I_2^- , which has been measured in Neumark's group.⁹ The experiments probe the rapid dissociation that takes place upon photoexcitation to the repulsive A' state. The experimental and simulated spectra shown in Fig. 2 demonstrate the good agreement we obtain. In both simulations and experiment, a broad band peaked near 1.9 eV at $t=0$ shifts rapidly in about 200 fs over to the spectrum of I^- as the I_2^- dissociates. The spectra evolve only slightly after 200 fs, suggesting that dissociation is essentially complete by then: the I-I separation is 5.4 Å at 200 fs in the simulation. The band shapes at early times are sensitive to the convoluted laser pulse width, which at 200 fs is broad compared to the dynamics being probed. The transient signal at high electron kinetic energy (>2.0 eV) is also sensitive to the inclusion of the entire manifold of I_2 product states. The previous simulation of the experiment⁹ failed to reproduce the high energy transients, probably because it included only the X , A , and A' states of I_2 .

$I_2^- Ar_6$ also dissociates rapidly upon photoexcitation, but the argon solvent atoms cause significant shifts in the observed spectra. As shown in Fig. 3(a), the experimental and simulated spectra agree well, although there are greater discrepancies at early times than seen in the bare ion spectra. Figure 3(b) shows typical cluster configurations during the dissociation along with the localization of the negative charge, and Fig. 3(c) shows the evolution of main peak position. As in the bare ion, the peak shifts rapidly during the first 200 fs toward lower electron kinetic energy as the I_2^- bond dissociates. In the simulations, the argon atoms cluster

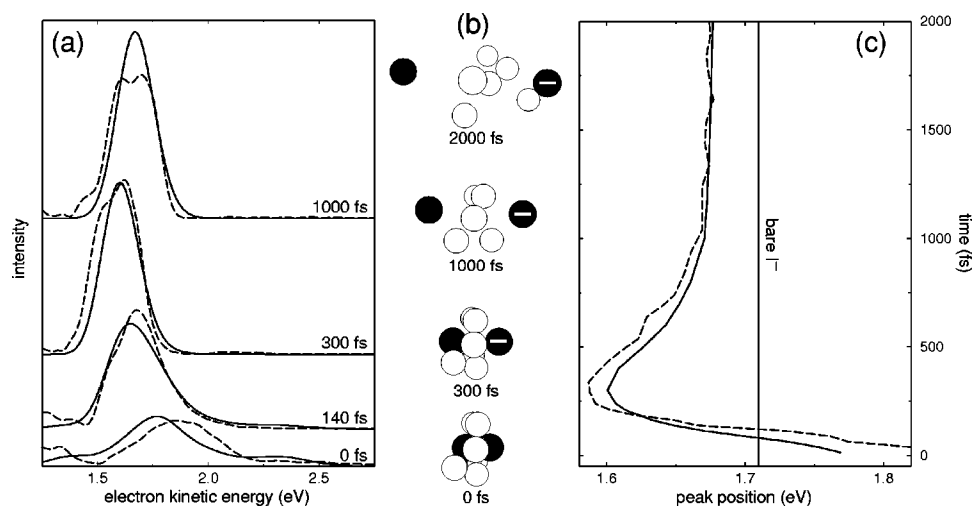


FIG. 3. Time-dependent photoelectron spectra of $I_2^- Ar_6$ with trajectory snapshots. Spectra at several pump-probe delay times are shown in (a), where solid lines are simulation results and dashed lines are experimental results from Ref. 19. The full width half maximum convoluted pulse width and detector width are 205 fs and 0.150 eV. The snapshots in (b) illustrate a typical trajectory with argon atoms in white and iodine atoms in black. The minus sign on the right iodine atom at $t \geq 300$ fs indicates charge localization on the initially less solvated iodine (see Ref. 14). The position of the main peak in the spectrum is plotted in (c) showing the large shift induced by the argon atoms at 300 fs.

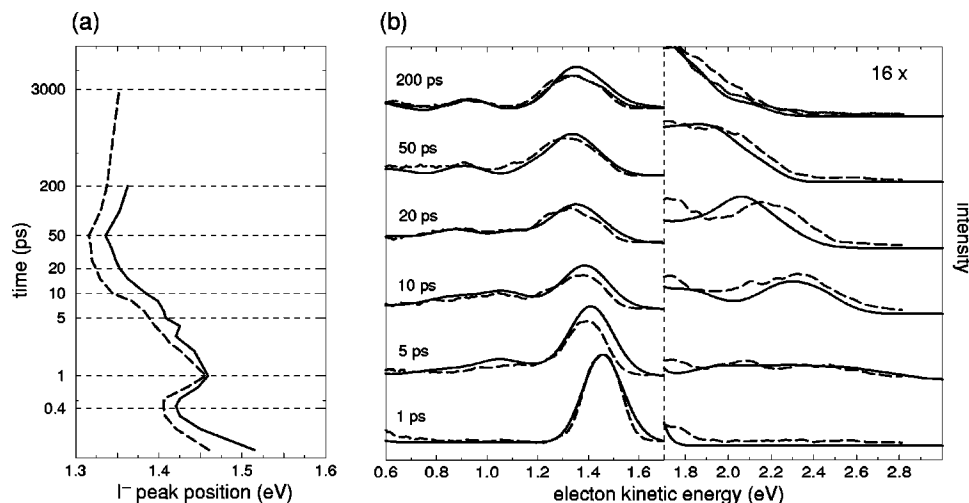


FIG. 4. Time-dependent photoelectron spectra of $I_2^- Ar_{20}$. Solid lines are simulation results and dashed lines are experimental results from Ref. 19. The position of the main peak is shown in (a) as a function of the pump-probe delay time. Full spectra at a series of delay times are shown in (b) where the right panel shows the high energy tail due to detachment from the X state of I_2^- . The dotted lines show the experimental spectrum at 3 ns. The full width half maximum convoluted pulse width and detector resolution width are 250 fs and 0.150 eV.

about the waist of I_2^- having little effect on the dissociating ion. By 300 fs the I–I separation is 6.4 Å, but the argon atoms have moved only slightly. Because the argon cluster remains largely intact, it exerts a shift of just over 100 meV in the peak position, corresponding to the shift observed in cold $I^-(Ar)_{4-5}$ clusters. By itself, this might suggest that $I^-(Ar)_{4-5}$ clusters are somehow formed as an intermediate in the dissociation, followed by rapid evaporation of argon atoms.¹⁹ In our simulation, however, dissociation is direct, with the argon atoms barely moving on the time scale of the peak shift. As the dissociation continues, only 1–2 argon atoms on average catch the escaping ion, and the peak rapidly moves to higher electron kinetic energy, nearly attaining its asymptotic value by 1 ps. There is a slight drift after 1 ps due to the gradual evaporation of argon from clusters in which more than 1 argon atom catch I^- .

The time-dependent photoelectron spectra of $I_2^- Ar_{20}$ probe the dynamics of dissociation and recombination processes that evolve over multiple time scales and potential surfaces. In both experiment and simulation, no dissociated products are observed for this cluster size, and recombination may occur in either the X or A states of I_2^- . In addition to probing the early dynamics of dissociation, the photoelectron spectra reveal the time scales for recombination into these states and the subsequent time required for vibrational and solvent relaxation. Figure 4(a) shows the evolution of the main spectral peak. Up to 1 ps, the motion of the peak is similar to $I_2^- Ar_6$, but the magnitude of the shift is much larger due to the greater number of solvent atoms. Unlike in $I_2^- Ar_6$, the shift toward higher electron kinetic energy between 0.4 and 1.0 ps is due to heating and evaporation of the argon atoms as the dissociating iodine atoms collide with the solvent cage. The simulations indicate that about 3–4 argon atoms are evaporated from the cluster during the initial dissociation event. By 1 ps a substantial fraction of the trajectories have begun to recombine, and between 1 and 5 ps the main peak shifts toward lower energy and diminishes in

intensity as two major new features appear in the spectrum at lower and higher energies [see Fig. 4(b)]. The simulations show that the new features are due to recombination in the X state that opens up photoelectron transitions to the X state of I_2^- . There is good agreement between the experiment and simulation for both the shapes and positions of these new bands. The appearance and growth of the bands provide an estimate of the time required for electronic relaxation and recombination to occur in the X state of I_2^- —about 5–10 ps. Most of the trajectories in the simulation that recombine in the X state do so between 3 and 5 ps, and all have recombined by 15 ps.

Subsequent evolution of the high energy band arises from vibrational relaxation in the X state I_2^- , which occurs rapidly in the first 10–20 ps after recombination, but stretches out over several hundred picoseconds in both the experiment and simulation. This band narrows and shifts to lower energy as I_2^- relaxes in the X state well, increasing the energetic gap for photodetachment to the X state of I_2^- . Figure 5(a) displays the ensemble average of the I_2^- total internal energy following electronic relaxation to the X state along with the average number of argon atoms remaining in the cluster. During the first 20 ps, about 80% of the initial vibrational energy is transferred into the solvent, which undergoes rapid evaporation to dissipate the energy. The rate of evaporation decreases dramatically below about $n = 5$, so that the solvent can no longer dissipate excess energy quickly and thus the rate of vibrational relaxation also slows. Vibrational relaxation is not complete in either the experiment or simulation even by 200 ps, a result reflecting the dynamics of evaporation from the small clusters near the bottom of the well rather than the characteristic ability of the argon solvent to absorb energy from the excited solute. In a pump-probe experiment on $I_2^- Ar_{20}$ Vorsa *et al.*⁸ have reported a time constant of 130 ps for the absorption recovery, which probably also reflects this slow vibrational relaxation at the bottom of the X state well.

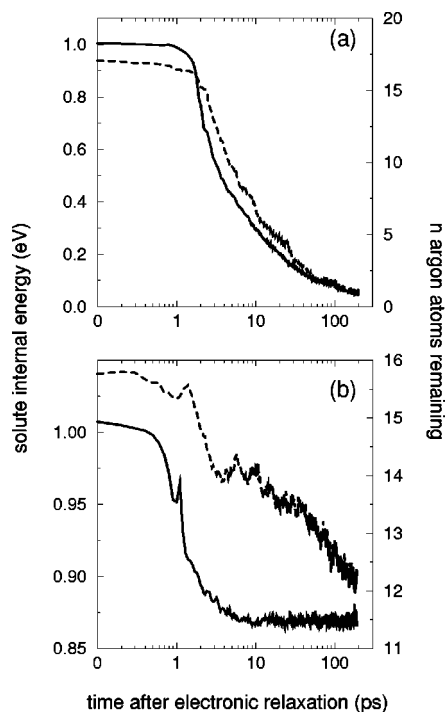


FIG. 5. Vibrational relaxation and solvent evaporation in $I_2^-Ar_{20}$ following electronic relaxation to the (a) the ground X state and (b) the excited A state. The solute internal energy, referenced to the bottom of the X state well, is shown by the solid line, and the number of solvent atoms remaining in the cluster, defined as inside a radius of 6.0 Å from either iodine atom, is indicated by the dashed line.

The experimental and simulated spectra at high energies track each other, although not as closely at longer times, probably indicating that the rates of vibrational relaxation do not match exactly. The experimental spectra reflect a somewhat slower rate of vibrational relaxation than the simulations, which may be expected given that the simulations overestimate the $I^- \cdots Ar$ interaction by about 10%. In the simulations I_2^- can impart somewhat more vibrational energy to the solvent before the solvent atoms lose their ability to absorb the energy effectively. The experimental spectrum at 3 ns, shown by the dotted line in Fig. 4(b), demonstrates that upon further vibrational relaxation the experimental spectrum more closely resembles the simulated spectrum at 200 ps. The observed differences in the spectra at 200 ps correspond to differences in the vibrational energy of 2–3 vibrational quanta, or about 40 meV.

The evolution of the main spectral peak, plotted in Fig. 4(a), follows the recombination and subsequent vibrational relaxation of I_2^- in the excited A state. This band loses intensity after 1 ps as about 40% of the ensemble recombines in the X state, where the photoelectron transitions are shifted to higher and lower energies. The position of the peak shifts to lower energy as the remainder of the ensemble recombines in the A state. The shape and position of the I^- band are not sensitive to the vibrational energy of the much shallower A state well, so the vibrational relaxation is not reflected in the spectra. The simulations reveal, however, that it takes only a few ps following recombination in the A state for I_2^- to lose nearly all of its vibrational energy, as shown in Fig. 5(b).

The peak continues to shift to lower energy out to about 50 ps, after which there is a slight shift to higher energy. Some of the shift out to 50 ps probably arises from overlap with bands from X state detachment, which continues to change on this time scale. By simulating the bands separately, however, we determined that some of the shift occurs even in the absence of overlap, because the recombination time in the A state is twice as long on average as in the X state, with recombination in some trajectories taking as long as 40 ps. The shift in the peak does not reach its maximal value until all of the trajectories that recombine in the A state have done so. The slow shift to higher energy after 50 ps reflects the continuing evaporation of argon atoms [see Fig. 5(b)], dissipating the remaining excess energy of the clusters. The main band at long times is much broader than the experimental energy resolution, resulting from detachment to all of the different low-lying states of I_2^- . These states significantly affect the shape of the spectrum at both short and long times.

IV. CONCLUSIONS

The $I_2^-Ar_6$ simulations provide a clearer picture of the dissociation than experiments alone were able to provide. Dissociation occurs directly, and the transient shifts in the photoelectron spectra reflect the breaking of the I_2^- bond, followed by the escape of I^- from the neutral solvent cluster. In $I_2^-Ar_{20}$ the dissociated atoms recombine, and the simulations confirm the interpretation of the experimental shifts as arising from recombination in both the X and A states of I_2^- , followed by vibrational relaxation. The agreement between the model and experiment for the time scales of these processes suggests that the simulations accurately depict the course of a chemical reaction evolving over several different electronic potential surfaces with strong coupling to a solvent. The discussion presented here also demonstrates the importance of modeling in conjunction with the interpretation of experimental results for these systems. In the future, nonadiabatic molecular dynamics simulations coupled with semiempirical Hamiltonian models should provide a useful tool for examining the dynamics of many reactions involving the excited states of charged species in the condensed phase.

ACKNOWLEDGMENTS

We would like to thank Professor D. Neumark, B. J. Greenblatt, and M. T. Zanni for helpful discussions and sharing their data with us prior to publication. We also thank N. Delaney and Dr. P. Maslen for their contributions to this project. This work was supported by the National Science Foundation under Grants No. CHE-92-17693 and PHY-95-12150, and by the National Center for Supercomputing Applications (NCSA) under Grant No. CHE97-0015N for computing time on the Silicon Graphics Power ChallengeArray at the NCSA, University of Illinois at Urbana-Champaign.

¹M. L. Alexander, M. A. Johnson, N. E. Levinger, and W. C. Lineberger, *Phys. Rev. Lett.* **57**, 976 (1986).

²M. L. Alexander, N. E. Levinger, M. A. Johnson, D. Ray, and W. C. Lineberger, *J. Chem. Phys.* **88**, 6200 (1988).

³D. Ray, N. E. Levinger, J. M. Papanikolas, and W. C. Lineberger, *J. Chem. Phys.* **91**, 6533 (1989).

- ⁴J. M. Papanikolas *et al.*, *J. Phys. Chem.* **95**, 8028 (1991).
- ⁵J. M. Papanikolas *et al.*, *J. Chem. Phys.* **99**, 8733 (1993).
- ⁶M. E. Nadal, P. D. Kleiber, and W. C. Lineberger, *J. Chem. Phys.* **105**, 504 (1996).
- ⁷V. Vorsa, P. J. Campagnola, S. Nandi, M. Larsson, and W. C. Lineberger, *J. Chem. Phys.* **105**, 2298 (1996).
- ⁸V. Vorsa, S. Nandi, P. J. Campagnola, M. Larsson, and W. C. Lineberger, *J. Chem. Phys.* **106**, 1402 (1997).
- ⁹B. J. Greenblatt, M. T. Zanni, and D. M. Neumark, *Chem. Phys. Lett.* **258**, 523 (1996).
- ¹⁰L. Perera and F. G. Amar, *J. Chem. Phys.* **90**, 7354 (1989). These authors simulated photodissociation of Br_2^- using a classical model for charge localization and emphasized the importance of charge switching.
- ¹¹P. E. Maslen, J. M. Papanikolas, J. Faeder, R. Parson, and S. V. O'Neil, *J. Chem. Phys.* **101**, 5731 (1994).
- ¹²J. M. Papanikolas, P. E. Maslen, and R. Parson, *J. Chem. Phys.* **102**, 2452 (1995).
- ¹³V. S. Batista and D. F. Coker, *J. Chem. Phys.* **106**, 7102 (1997).
- ¹⁴J. Faeder, N. Delaney, P. Maslen, and R. Parson, *Chem. Phys. Lett.* **270**, 196 (1997).
- ¹⁵N. Delaney, J. Faeder, P. E. Maslen, and R. Parson, *J. Phys. Chem. A* **101**, 8147 (1997).
- ¹⁶V. S. Batista and D. F. Coker, *J. Chem. Phys.* **105**, 4033 (1996).
- ¹⁷V. S. Batista and D. F. Coker, *J. Chem. Phys.* **106**, 6923 (1997).
- ¹⁸A. Buchachenko and N. Stepanov, *J. Chem. Phys.* **104**, 9913 (1996).
- ¹⁹B. J. Greenblatt, M. T. Zanni, and D. M. Neumark, *Science* **276**, 1675 (1997).
- ²⁰P. E. Maslen, J. Faeder, and R. Parson, *Mol. Phys.* (submitted).
- ²¹P. E. Maslen, J. Faeder, and R. Parson, *Chem. Phys. Lett.* **263**, 63 (1996).
- ²²M. T. Zanni, T. R. Taylor, B. J. Greenblatt, B. Soep, and D. M. Neumark, *J. Chem. Phys.* **107**, 7613 (1997).
- ²³C. G. Gray and K. E. Gubbins, *Theory of Molecular Fluids* (Clarendon, Oxford, 1984), Vol. 1.
- ²⁴K. T. Tang and J. P. Toennies, *J. Chem. Phys.* **80**, 3726 (1984).
- ²⁵Y. Zhao, I. Yourshaw, G. Reiser, C. C. Arnold, and D. M. Neumark, *J. Chem. Phys.* **101**, 6538 (1994).
- ²⁶I. Yourshaw, Y. Zhao, and D. M. Neumark, *J. Chem. Phys.* **105**, 351 (1996).
- ²⁷D. R. T. Appadoo *et al.*, *J. Chem. Phys.* **104**, 903 (1996), and references therein.
- ²⁸J. Tellinghuisen, *J. Chem. Phys.* **82**, 4012 (1985).
- ²⁹K. S. Viswanathan and J. Tellinghuisen, *J. Mol. Spectrosc.* **101**, 285 (1983).
- ³⁰S. Churassy, F. Martin, R. Bacis, J. Vergès, and R. W. Field, *J. Chem. Phys.* **75**, 4863 (1981).
- ³¹C. Teichteil and M. Pelissier, *Chem. Phys.* **180**, 1 (1994).
- ³²J. C. Tully, *J. Chem. Phys.* **93**, 1061 (1990).
- ³³S. Hammes-Schiffer and J. C. Tully, *J. Chem. Phys.* **101**, 4657 (1994).
- ³⁴E. R. Bittner and P. J. Rossky, *J. Chem. Phys.* **103**, 8130 (1995).
- ³⁵B. J. Schwartz, E. R. Bittner, O. V. Prezhdo, and P. J. Rossky, *J. Chem. Phys.* **104**, 5942 (1996).
- ³⁶R. S. Mulliken, *J. Chem. Phys.* **55**, 288 (1971).